High-quality $SnSe_2$ single crystal: Electronic and thermoelectric properties

*Anh-Tuan Pham[1], Thi Hoa Vu[1], Chang Cheng[2], Thi Ly Trinh[1], Ji-Eun Lee[3,4], Hyejin Ryu[3], Choongyu Hwang[4], Sung-Kwan Mo[5], Jungdae Kim[1], Li-dong Zhao[2], Anh-Tuan Duong[6**], and Sunglae Cho[1*]*

[1]Department of Physics and Energy Harvest-Storage Research Center, University of Ulsan, Ulsan 44610, Republic of Korea

[2]School of Materials Science and Engineering, Beihang University, Beijing 100191, China

[3]Center for Spintronics, Korea Institute of Science and Technology (KIST), Seoul 02792, Republic of Korea

[4]Department of Physics, Pusan National University, Busan 46241, Republic of Korea

[5]Advanced Light Source, Lawrence Berkeley National Laboratory, Berkeley, CA 94720, USA

[6]Phenikaa Research and Technology Institute (PRATI) and Faculty of Materials Science and Engineering, Phenikaa University, Hanoi 12116, Vietnam

ABSTRACT

The high-quality $SnSe_2$ single crystal was successfully synthesized using the temperature gradient method. N-type characteristic and strong anisotropic transport properties of $SnSe_2$ single crystal were exhibited between ab-plane and c-axis. At 673 K, the power factor (PF) value along ab-plane is $3.43\ \mu W\ cm^{-1}\ K^{-2}$ while it along c-axis is $0.92\ \mu W\ cm^{-1}\ K^{-2}$. The ratio between thermal conductivities along ab-plane (κ_{ab}) and along c-axis (κ_c) is 7.6 order at 300 K, while as at 673 K, this value about 5.6. The thermoelectric figure of merit *ZT* along c-axis (0.15) is higher than that (0.1) along the ab-plane, according to the ultra-lower out-of-plane thermal conductivity. The electronic band structure results, which were examined by angle-resolved photoemission spectroscopy (ARPES) predicted the potential of improving thermoelectric performance of $SnSe_2$ single crystal by electron doping.

Keywords: *Thermoelectric material, single crystal, $SnSe_2$, ultra-low thermal conductivity, ARPES.*

I. INTRODUCTION

Recently, thermoelectric materials, which directly convert waste heat into electricity, have increasingly attracted attention. The thermoelectric performance is evaluated by the dimensionless thermoelectric figure of merit, $ZT = \frac{S^2\sigma T}{\kappa}$, where S, σ, T, and κ represent the Seebeck coefficient, electrical conductivity, absolute temperature, and thermal conductivity, respectively[1,2]. To reach excellent performance as a commercial product, S and σ should stay at high value, while as κ remains low. Since these three transport coefficients are inter-dependent, it is difficult to optimize ZT value. There are typical ways to improve ZT value such as enhancing the power factor $S^2\sigma$ via optimizing the carrier concentration n and mobility μ or suppressing the lattice thermal conductivity κ_L by introducing the scattering centers. As a result, there are currently only a few materials used for commercial applications.

In layered structure materials, the difference in bonding mechanism between in-plane and out-of-plane leads to unique electronic and thermal transport properties. Among them, layered chalcogenide crystals possessing strong intra-layer covalent bonding and noticeable weak inter-layer van der Waals bonding, such as Bi_2Te_3 and Sb_2Te_3, are by far recognized as good thermoelectric materials at around room temperature. In addition, layered SnSe with the weak cross-plane covalent bonds, has been reported with in-plane ZT = 2.6 at 923 K in p-type SnSe[3], and ZT = 2.2 at 733 K in Bi-doped n-type SnSe[4]; out-of-plane ZT = 2.8 at 773 K in Br-doped n-type SnSe[5].

In the layered structure materials family, Tin diselenide ($SnSe_2$) possesses the CdI_2-type hexagonal structure with space group $P\bar{3}m1$, which is formed by a van der Waals bonding between Sn-Se-Sn slabs along out-of-plane direction (c-axis). Lattice parameters of $SnSe_2$ are a = 3.811 Å and c = 6.137 Å[6]. $SnSe_2$ has yet confirmed belonging to n-type semiconductor with indirect band gap of 0.97 eV[7], which was considered as applications such as phase-change memory, optoelectronic devices, field-effect transistors (FETs), and gas sensor devices[8–12]. Recently, $SnSe_2$ has attracted interest from scientists due to its ultralow thermal conductivity. Some theoretical calculations have predicted that thermoelectric properties of $SnSe_2$

are significantly influenced by carrier concentration. *ZT* value of p-type $SnSe_2$ monolayer can be obtained up to 0.94 at 600 K with carrier concentration around 10^{19} cm^{-3}, while that of n-type $SnSe_2$ is around 0.8 with carrier concentration around 10^{20} cm^{-3} [13]. Ding *et al*. predicted that at 800 K, *ZT* values of n-type $SnSe_2$ are 0.01, 0.2, 1.1, and 2.95 with carrier concentrations of 10^{17}, 10^{18}, 10^{19}, and 10^{20} cm^{-3}, respectively[14]. By doping Cl, Xu *et al.* achieved $ZT = 0.4$ at 673 K in $SnSe_{1.88}Cl_{0.12}$ polycrystals[15]. By doping Ag, Li *et al.* also obtained $ZT = 0.4$ in $Sn_{0.99}Ag_{0.01}Se_2$ at 773 K[16]. By substituted Br into Se sites of $SnSe_2$, Wu *et al*. improved *ZT* to 0.6 at 750 K[17].

Based on potential applications of $SnSe_2$ crystal, the synthesis of high-quality $SnSe_2$ single crystal is beneficial in studying the intrinsic thermoelectric properties. In this article, high crystalline quality $SnSe_2$ has been grown by simple temperature gradient method and has been studied anisotropic thermoelectric transport properties. The thermoelectric performance of $SnSe_2$ single crystal shows better than the results on polycrystalline. Besides, the ARPES results show the potential for improving thermoelectric performance by electron doping.

II. EXPERIMENT

$SnSe_2$ single crystal was grown by the temperature gradient method[18]. First, high purity (5N) Se and Sn powders with the mole ratio of 2:1 were weighed and sealed in quartz ampoule under vacuum ($<10^{-4}$ Torr). Then, the ampoule was heated to 750 °C (60 °C h^{-1}) and soaked for 10 hours. Finally, the temperature was gradually cooled with a rate of 1 °C h^{-1} to 550 °C, then rapidly dropped to room temperature (50 °C h^{-1}). A high-quality $SnSe_2$ crystal with sizes of 14 mm diameter × 30 mm length was obtained. The crystal structure was studied by means of X-ray diffraction (XRD). Field Emission Scanning Electron Microscopy (FE-SEM) and Energy Dispersive X-ray Spectroscopy (EDS) were used to observe the layer morphology and stoichiometry of the samples, respectively.

To study the thermoelectric properties in both directions, parallel (ab-plane) and perpendicular (c-axis) to the layered plane, bar-shaped samples used to measure the Seebeck coefficient and electrical

conductivity, and disk-shaped samples used to measure thermal diffusivity were cut into a precise size 3 x 3 x 10 mm^3 and 13 x 13 x 1 mm^3, respectively. Seebeck coefficient and electrical conductivity were determined simultaneously in an Argon environment to prevent oxidation and evaporation. Hall measurement was studied in various temperatures from 300 to 673 K via the van der Pauw method under a reversible magnetic field of 0.7 T. The laser flash diffusivity method (LFA-457, NETZSCH, Germany) was used to evaluate the thermal diffusivity D. The heat capacity was determined from the measured values of Wiedemeier *et al*[19]. by $C_{\mathrm{p}} = 73.39 + 1.15 \times 10^{-2} T - 1.92 \times 10^{5} T^{-2}\ (J\,K^{-1}\,mol^{-1})$ with the uncertainty of 1% for $SnSe_2$. The total thermal conductivity was obtained following the formula $\kappa_{\mathrm{tot}} = D.C_{\mathrm{p}}.\rho$, with ρ is the mass density measured by the Archimedes' principle at 300 K. The lattice thermal conductivity κ_L was obtained by subtracting the electronic contribution ($\kappa_{\mathrm{e}} = LT/\rho$) from the total thermal conductivity κ_{tot}, where the Lorenz number[20] ($L \sim [1.5 + exp\,(-\frac{|S|}{116})] \times 10^{-8}\,W\,\Omega\,K^{-2}$) was estimated from the Seebeck coefficient data. Transport property measurements (S, σ, and κ) were conducted from room temperature to 673 K, with the uncertainty of each being ~5%. Angle-resolved photoemission spectroscopy (ARPES) was performed at the Beamline 10.0.1, Advanced Light Source, using photon energy 55 eV. The measurements were made under base pressure below 4 x 10^{-11} Torr at 30 K.

III. RESULTS AND DISCUSSION

By using temperature gradient method, we have been successfully grown high-quality $SnSe_2$ single crystals. Figure 1a describes the real image of the grown samples with cleaved shiny surfaces. EDS measurement indicates the proportion of Se and Sn to be 2:1, as shown in Figure 1b. The surface of cleaved $SnSe_2$ single crystal was observed by FE-SEM. The results exhibited a clear surface and a lamellar microstructure with an average thickness of a few tens nanometer, as shown in Figure 1c. For STM (Scanning Tunneling Microscopy) studies, the sample was cleaved in-situ to obtain clean surfaces of

$SnSe_2$ single crystal. High resolution STM image in Figure 1d proved the appearance of hexagonal structure of Se on the surface of $SnSe_2$.

The XRD result of cleaved $SnSe_2$ single crystal without any impure peaks has been shown in Figure 2a. Compared with JCPDS PDF 89-3197 data, all diffraction peaks belong to the hexagonal $SnSe_2$ structure and the patterns showed only (*00l*) peak group. Lattice parameters of $SnSe_2$ single crystal were calculated from powder XRD data (as shown in Figure 2b) with a $CuK\alpha_1$ radiation; a =3.808 Å and c = 6.129 Å are comparable with earlier reported. The calculated mass density of the grown $SnSe_2$ single crystal by lattice parameters is 5.966 g/cm^{-3}, which agreed well with that of the directly measured one, 5.937 ± 0.11 g/cm^{-3}.

Figure 3a represents the temperature dependence of carrier concentration $n(T)$ which is obtained from Hall measurement by using formula $\frac{V_H}{I} = \frac{1}{ned}H$, where V_H is Hall voltage, I is the current, n is the number of carriers, e is electrical charge, H is magnetic field, and d is sample thickness. As increasing temperature, n gradually increases from $2.26 \times 10^{18}\, cm^{-3}$ at 300 K to $3.37 \times 10^{18}\, cm^{-3}$ at 473 K and then dramatically increases up to $3.05 \times 10^{19}\, cm^{-3}$ at 673 K. The number of carrier at 300 K is one order of magnitude higher than that of the previous reported single crystal by Julien *et al*. prepared by the Bridgman technique, while the electron mobility along ab-plane, $\mu = 31.6\, cm^2\, V^{-1}\, s^{-1}$ (Figure 3b), is quite similar[6]. The mobility along both directions decreases sharply with temperature and obeys the trend of $T^{-3/2}$, pointing out that the acoustic phonon scattering is the major contribution. These results are reasonable compared with previous works on single crystals and polycrystals of $SnSe_2$. However, the mobility value in single crystal is much higher than those in polycrystalline samples[6,21–23]. Thermoelectric properties of $SnSe_2$ single crystal have been measured along cleaved surface (ab-plane) and perpendicular cleaved surface (c-axis) from 300 to 673 K, as shown in Figure 4. Electrical conductivity showed semiconducting behavior. However, measurement results along cleaved surface and perpendicular cleaved surface are different due to anisotropic transport properties of this material. Especially at above 500 K,

electrical conductivity along the cleaved plane (σ_{ab}) increases up to 35.97 S cm^{-1} at 673 K caused by the rapid rise of carrier concentration. Seebeck coefficient along and perpendicular to cleaved surface follows a similar trend, as shown in Figure 4b. From room temperature to 500 K, $SnSe_2$ single crystal exhibited the metallic transport behavior. This transport behavior can also be observed in Figure 3b when the carrier mobility forms a sharp degradation, in contrast, the carrier concentration slightly increases along with the temperature. As generally expected, Seebeck coefficients slowly rise with the temperature, which corresponds to the fall of electrical conductivity. At above 500 K, sample shows thermally activated transport behavior. So, both electrical conductivity and Seebeck coefficient show an opposite trend compared to those in the lower temperatures. Figure 4c shows the thermoelectric power factor ($PF = S^2\sigma$) along both directions. Maximum *PF* along cleaved plane (3.47 μW cm^{-1} K^{-2}) is larger than that along c-axis direction (0.97 μW cm^{-1} K^{-2}) owing to the relatively big difference in electrical conductivities between the two directions. Furthermore, its anisotropy becomes stronger with temperature. Because of the limitation of material thermal stability, it is impractical to carry out the experiment at higher temperatures. Therefore, peak electrical conductivities are not obtained in this temperature range, and the highest value is around 35.97 S cm^{-1} at 673 K.

Temperature-dependent total thermal conductivities (κ_{tot}) along and perpendicular cleaved surface are shown in Figure 4d. The data revealed the lattice thermal conductivity accounts for 98 % of κ_{tot}; phonon transport contributed to most total heat transfer in $SnSe_2$. From the inset, the lattice thermal conductivities (in-plane & out-of-plane) decrease as T^{-1} along with temperature, this could result from the anharmonic phonon-phonon interactions. In addition, the obtained in-plane thermal conductivity (κ_{ab}) is significantly larger than that out of plane one (κ_c) at all temperatures. At 300 K, we found κ_{ab} = 6.9 W m^{-1} K^{-1} which is nearly eight times higher than κ_c = 0.9 W m^{-1} K^{-1}. The ratio κ_{ab}/κ_c = 7.6 indicates strong anisotropy in thermal conductivity of $SnSe_2$. Moreover, at 673 K, the out of plane κ_c even drops to an ultralow value of 0.43 W m^{-1} K^{-1}. The large anisotropy in thermal transport properties is well explained from crystal

structure and bonding characters of $SnSe_2$. This is a consequence of ultraweak van der Waals forces among layers compared with the intralayer covalent bonding. These values agree well with both previous experimental[21] and theoretical studies[22,23].

ZT values along and perpendicular cleaved surface have been shown in Figure 5. *ZT* values of both directions increase with temperature. Ultra-low out-of-plane thermal conductivity is the cause of higher ZT_c value compared to that along ab-plane ZT_{ab}. We determine the maximum *ZT* value of $SnSe_2$ single crystal along c-axis direction is 0.15 at 673 K, while that along ab-plane is 0.1. Note that, in previous experiment reports, *ZT* value of un-doped $SnSe_2$ polycrystal is usually smaller 0.05[9,10]. In two theoretical calculations by Li *et al*. and Ding *et al.*, *ZT* value of monolayer and single crystal of $SnSe_2$ are strongly dependent on carrier concentration. In n-type $SnSe_2$ monolayer, *ZT* value at 900 K with electron concentration of 10^{18} cm^{-3} is 0.1 and it increases up to 1.1 with *n* of 10^{20} cm^{-3}. In the $SnSe_2$ single crystal, *ZT* value at 800 K is 0.15 with $n \approx 10^{18}$ cm^{-3} and increases up to 2.95 with $n \approx 10^{20}$ cm^{-3} [14,27].

To study the relation between *ZT* and electronic band structures, we analyze the electronic band structure of $SnSe_2$ single crystals using ARPES. Overall band structure obtained from ARPES experiments is consistent with the reported theoretical results[28,29]. The position of the valence band maximum (VBM) of pristine $SnSe_2$ is 1.36 eV below Fermi energy (E_F) with no photoemission intensity near E_F, implying that $SnSe_2$ is an intrinsic *n*-type semiconductor (Figure 6a, b). The constant energy contour at VBM shows a flower-like shape, indicating three-fold rotational symmetry of $SnSe_2$. By potassium (K) doping, $SnSe_2$ is electron-doped so that conduction bands are clearly revealed at the M point (Figure 6c), which is comparable with the earlier calculation result[28]. The extracted effective masses from the conduction band of $SnSe_2$ are $m^*_{\Gamma-M} = (2.63 \pm 0.12)m_e$ and $=m^*_{K-M} = (1.56 \pm 0.10)m_e$ (Figure 6d), which are similar to the theoretical value[30]. Note that the ARPES measurement is performed at 30 K to illustrate the band structure clearly, while most of the discussion in literatures are performed at 300 – 800 K where the thermoelectric applications are most relevant[26]. Therefore, it is better to focus on providing useful

information on how the added electrons would populate conduction band by potassium doping on the surface rather than looking for direct signature of conduction band in our low temperature ARPES results.

To achieve high *ZT* of a thermoelectric material, band engineering is proposed as an effective strategy, but the resulting enhancement is often subtle due to the competition among the factors constituting the *ZT* value. *ZT* is determined by electrical conductivity, Seebeck coefficient, and thermal conductivity which depend on charge carrier concentration (*n*) in a conflicting manner suggesting that optimizing *n* is a significant strategy for enhancing *ZT*. For $SnSe_2$, *ZT* maximizes when *n* is around 10^{20} cm^{-3} which is higher than the *n* of pristine $SnSe_2$ (~10^{18} cm^{-3})[26]. Our ARPES data clearly shows that electron doping fills up the conduction bands rather than forming the in-gap states resulting in the metallic band character (Figure 6c, d)), which is in contrast to the semiconducting band character of pristine $SnSe_2$ (Figure 6a, b). This proposes that thermoelectric properties of tin diselenide can be improved by enhanced *n* yielding the changes in the band character from semiconducting with *n* ~10^{18} cm^{-3} to metallic with *n* ~10^{20} cm^{-3}, induced by electron doping.

According to the calculations of the partial and total density of state (DOS) for $SnSe_2$[31], the Sn 4*p* orbitals mainly contribute to the lowest conduction bands, in which the contribution of Se $4p_z$ is less than that of Se $4p_x$ and $4p_y$. This leads to the superiority of in-plane electrical conductivity compared to the out-of-plane direction. However, with increasing carrier concentration by heavy donor doping, the carriers will fill Se $4p_z$ partially when Se $4p_x$ and $4p_y$ are already filled, leading to a steady increase in out-of-plane electrical conductivity. Thus, theoretical calculations support our higher ZT_c of 0.15 along the *c*-axis, compared to ZT_{ab} of 0.1 in the *ab*-plane, indicating better out-of-plane thermoelectric properties. We expect the significant boost of thermoelectric performance in out-of-plane ZT_c, when $SnSe_2$ can be heavily electron-doped.

IV. CONCLUSIONS

In summary, we synthesized a high-quality $SnSe_2$ single crystal using the temperature gradient method. The bulk material showed strong anisotropy in both electrical and thermal conductivity. An ultralow thermal conductivity κ_c= 0.43 W m^{-1} K^{-1} was obtained at 673 K, which creates a favorable condition to enhance thermoelectric performance. The out-of-plane thermoelectric figure of merit (ZT_c) value is 0.15 at 673 K, which is higher than that in-plane because of the lower out-of-plane thermal conductivity of $SnSe_2$ single crystal. ARPES data predicts that the power factor can be significantly improved via electronic doping.

AUTHOR INFORMATION

Corresponding Author

*Email: slcho@ulsan.ac.kr (S.C.)

**Email: tuan.duonganh@phenikaa-uni.edu.vn (T.A.D.)

Author contributions

The manuscript was written through contributions of all authors. All authors have given approval to the final version of the manuscript.

ACKNOWLEDGEMENTS

This research is funded by the National Research Foundation of Korea [NRF-2019R1F1A1058473, NRF-2019R1A6A1A11053838, and NRF-2020K1A4A7A02095438] and Vietnam's National Foundation for Science and Technology Development (NAFOSTED) under grant number 103.02-2019.354.

H.R. and J.L. acknowledge the KIST Institutional Program (2E29410) and the NRF of Korea (MSIT; 2019K1A3A7A09033388 and NRF-2020R1A5A1104591). This research used resources of the Advanced Light Source, a U.S. DOE Office of Science User Facility under contract no. DE-AC02-05CH11231. C.H.

also acknowledges support from the National Research Foundation of Korea (NRF) grant funded by the Korea government (MIST; No. 2018R1A2B6004538 and 2020K1A3A7A09080369).

REFERENCES

(1) Tritt, T. M.; Subramanian, M. a. Thermoelectric Materials, Phenomena, and Applications : A Bird' s Eye View. *MRS Bull.* **2006**, *31* (March), 188–198. https://doi.org/10.1557/mrs2006.44.

(2) Gaultois, M. W.; Sparks, T. D.; Borg, C. K. H.; Seshadri, R.; Bonificio, W. D.; Clarke, D. R. Data-Driven Review of Thermoelectric Materials: Performance and Resource Considerations BT - Chemistry of Materials. *Chem. Mater.* **2013**, *25*, 2911–2920. https://doi.org/10.1021/cm400893e.

(3) Zhao, L.-D.; Lo, S.-H.; Zhang, Y.; Sun, H.; Tan, G.; Uher, C.; Wolverton, C.; Dravid, V. P.; Kanatzidis, M. G. Ultralow Thermal Conductivity and High Thermoelectric Figure of Merit in SnSe Crystals. *Nature* **2014**, *508* (7496), 373–377. https://doi.org/10.1038/nature13184.

(4) Duong, A. T.; Nguyen, V. Q.; Duvjir, G.; Duong, V. T.; Kwon, S.; Song, J. Y.; Lee, J. K.; Lee, J. E.; Park, S.; Min, T.; Lee, J.; Kim, J.; Cho, S. Achieving ZT=2.2 with Bi-Doped n-Type SnSe Single Crystals. *Nat. Commun.* **2016**, *7*, 13713. https://doi.org/10.1038/ncomms13713.

(5) Chang, C.; Wu, M.; He, D.; Pei, Y.; Wu, C. F.; Wu, X.; Yu, H.; Zhu, F.; Wang, K.; Chen, Y.; Huang, L.; Li, J. F.; He, J.; Zhao, L. D. 3D Charge and 2D Phonon Transports Leading to High Out-of-Plane ZT in n-Type SnSe Crystals. *Science (80-.).* **2018**, *360* (6390), 778–783. https://doi.org/10.1126/science.aaq1479.

(6) Julien, C.; Eddrief, M.; Samaras, I.; Balkanski, M. Optical and Electrical Characterizations of SnSe, SnS2 and SnSe2 Single Crystals. *Mater. Sci. Eng. B* **1992**, *15* (1), 70–72. https://doi.org/10.1016/0921-5107(92)90033-6.

(7) Domingo, G.; Itoga, R. S.; Kannewurf, C. R. Fundamental Optical Absorption in SnS2 and SnSe2. *Phys. Rev.* **1966**, *143* (2), 536–541. https://doi.org/10.1103/PhysRev.143.536.

(8) Chung, K.-M.; Wamwangi, D.; Woda, M.; Wuttig, M.; Bensch, W. Investigation of SnSe, SnSe2, and Sn2Se3 Alloys for Phase Change Memory Applications. *J. Appl. Phys.* **2008**, *103* (8), 083523. https://doi.org/10.1063/1.2894903.

(9) Li, M. O.; Esseni, D.; Nahas, J. J.; Jena, D.; Xing, H. G. Two-Dimensional Heterojunction Interlayer Tunneling Field Effect Transistors (Thin-TFETs). *IEEE J. Electron Devices Soc.* **2015**, *3* (3), 200–207. https://doi.org/10.1109/JEDS.2015.2390643.

(10) Roy, T.; Tosun, M.; Hettick, M.; Ahn, G. H.; Hu, C.; Javey, A. 2D-2D Tunneling Field-Effect Transistors Using WSe2/SnSe2 Heterostructures. *Appl. Phys. Lett.* **2016**, *108* (8). https://doi.org/10.1063/1.4942647.

(11) Rai, R. K.; Islam, S.; Roy, A.; Agrawal, G.; Singh, A. K.; Ghosh, A.; Ravishankar, N. Morphology Controlled Synthesis of Low Bandgap SnSe2 with High Photodetectivity. **2019**, *2* (0001), 870–877. https://doi.org/10.1039/c8nr08138g.

(12) Saha, S.; Banik, A.; Biswas, K. Few-Layer Nanosheets of n-Type SnSe 2. *Chem. - A Eur. J.* **2016**, *22* (44), 15634–15638. https://doi.org/10.1002/chem.201604161.

(13) Li, G.; Ding, G.; Gao, G. Thermoelectric Properties of SnSe2 Monolayer. *J. Phys. Condens. Matter* **2017**, *29* (1), 015001. https://doi.org/10.1088/0953-8984/29/1/015001.

(14) Ding, Y.; Xiao, B.; Tang, G.; Hong, J. Transport Properties and High Thermopower of SnSe2: A Full Ab-Initio Investigation. *J. Phys. Chem. C* **2017**, *121* (1), 225–236. https://doi.org/10.1021/acs.jpcc.6b11467.

(15) Xu, P.; Fu, T.; Xin, J.; Liu, Y.; Ying, P.; Zhao, X.; Pan, H.; Zhu, T. Anisotropic Thermoelectric Properties of Layered Compound SnSe2. *Sci. Bull.* **2017**, *62* (24), 1663–1668. https://doi.org/10.1016/j.scib.2017.11.015.

(16) Li, F.; Zheng, Z.; Li, Y.; Wang, W.; Li, J. F.; Li, B.; Zhong, A.; Luo, J.; Fan, P. Ag-Doped SnSe2 as a Promising Mid-Temperature Thermoelectric Material. *J. Mater. Sci.* **2017**, *52* (17), 10506–10516. https://doi.org/10.1007/s10853-017-1238-8.

(17) Wu, Y.; Li, W.; Faghaninia, A.; Chen, Z.; Li, J.; Zhang, X.; Gao, B.; Lin, S.; Zhou, B.; Jain, A.; Pei, Y. Promising Thermoelectric Performance in van Der Waals Layered SnSe 2. *Mater. Today Phys.* **2017**, *3*, 127–136. https://doi.org/10.1016/j.mtphys.2017.10.001.

(18) Choi, J.; Lee, H.; Kim, B.; Park, H.; Choi, S.; Hong, S. C.; Cho, S. Magnetic and Transport Properties of Mn-Doped Bi 2 Se 3 and Sb 2 Se 3. **2006**, *304*, 164–166. https://doi.org/10.1016/j.jmmm.2006.02.041.

(19) Wiedemeier, H.; Pultz, G.; Gaur, U.; Wunderlich, B. Heat Capacity Measurements of SnSe and SnSe2. *Thermochim. Acta* **1981**, *43* (3), 297–303. https://doi.org/10.1016/0040-6031(81)85187-8.

(20) Kim, H. S.; Gibbs, Z. M.; Tang, Y.; Wang, H.; Snyder, G. J. Characterization of Lorenz Number swith Seebeck Coefficient Measurement. *APL Mater.* **2015**, *3* (4), 1–6. https://doi.org/10.1063/1.4908244.

(21) Liu, M.; Zhang, J.; Xu, J.; Hu, B.; Sun, K.; Yang, Y.; Wang, J.; Du, B.; Zhang, H. The Crystallization, Thermodynamic and Thermoelectric Properties of Vast off-Stoichiometric Sn–Se Crystals. *J. Mater. Chem. C* **2020**. https://doi.org/10.1039/c9tc06903h.

(22) Shu, Y.; Su, X.; Xie, H.; Zheng, G.; Liu, W.; Yan, Y.; Luo, T.; Yang, X.; Yang, D.; Uher, C.; Tang, X. Modification of Bulk Heterojunction and Cl Doping for High-Performance Thermoelectric SnSe2/SnSe Nanocomposites. *ACS Appl. Mater. Interfaces* **2018**, *10* (18), 15793–15802. https://doi.org/10.1021/acsami.8b00524.

(23) Liu, M.; Zhang, J.; Xu, J.; Hu, B.; Liu, B.; Sun, K.; Yang, Y.; Wang, J.; Du, B. Phase Structure,

Phase Transition and Thermoelectric Properties of Pristine and Br Doped SnSe2. *J. Solid State Chem.* **2020**, *289* (April), 121468. https://doi.org/10.1016/j.jssc.2020.121468.

(24) Busch, G. Thermoelektrische Eigenschaften. **1961**, 359–368.

(25) Wang, H.; Gao, Y.; Liu, G. Anisotropic Phonon Transport and Lattice Thermal Conductivities in Tin Dichalcogenides SnS2 and SnSe2. *RSC Adv.* **2017**, *7* (14), 8098–8105. https://doi.org/10.1039/C6RA27761F.

(26) Ding, Y.; Xiao, B.; Tang, G.; Hong, J. Transport Properties and High Thermopower of $SnSe_2$: A Full Ab-Initio Investigation. *J. Phys. Chem. C* **2016**, acs.jpcc.6b11467. https://doi.org/10.1021/acs.jpcc.6b11467.

(27) Li, G.; Ding, G.; Gao, G. Thermoelectric Properties of $SnSe_2$ Monolayer. *J. Phys. Condens. Matter* **2017**, *29* (1), 015001. https://doi.org/10.1088/0953-8984/29/1/015001.

(28) Lochocki, E. B.; Vishwanath, S.; Liu, X.; Dobrowolska, M.; Furdyna, J.; Xing, H. G.; Shen, K. M. Electronic Structure of SnSe2 Films Grown by Molecular Beam Epitaxy. *Appl. Phys. Lett.* **2019**, *114* (9). https://doi.org/10.1063/1.5084147.

(29) Kim, S. Il; Hwang, S.; Kim, S. Y.; Lee, W.-J.; Jung, D. W.; Moon, K.-S.; Park, H. J.; Cho, Y.-J.; Cho, Y.-H.; Kim, J.-H.; Yun, D.-J.; Lee, K. H.; Han, I.; Lee, K.; Sohn, Y. Metallic Conduction Induced by Direct Anion Site Doping in Layered SnSe2. *Sci. Rep.* **2016**, *6*, 19733. https://doi.org/10.1038/srep19733.

(30) Rasmussen, F. A.; Thygesen, K. S. Computational 2D Materials Database : Electronic Structure of Transition-Metal Dichalcogenides and Oxides. **2015**. https://doi.org/10.1021/acs.jpcc.5b02950.

(31) Bletskan, D. I. Electronic Structure of 2H-SnSe2: Ab Initio Modeling and Comparison with

Experiment. *Semicond. Phys. Quantum Electron. Optoelectron.* **2016**, *19* (1), 98–108. https://doi.org/10.15407/spqeo19.01.098.

Figure captions

Figure 1. (a) Photo of samples, (b) EDS measurement data, (c) FE-SEM image, and (d) STM image of $SnSe_2$ single crystal.

Figure 2. Room temperature XRD patterns of (a) cleaved and (b) powdered $SnSe_2$.

Figure 3. Temperature dependence of (a) carrier concentrations and (b) carrier mobility of $SnSe_2$ single crystal.

Figure 4. Temperature-dependent thermoelectric transport properties along both directions. (a) Electrical resistivity $\sigma(T)$, (b) Seebeck coefficient $S(T)$, (c) power factor $S^2\sigma$, and (d) thermal conductivity $\kappa(T)$.

Figure 5. Temperature-dependent dimensionless figure of merit *ZT* of $SnSe_2$ along both directions.

Figure 6. The electronic band structure of pristine and potassium (K) doped $SnSe_2$ single crystal. (a) Constant energy contour of pristine $SnSe_2$ for the binding energy of -1.36 eV. (b) ARPES spectra of pristine $SnSe_2$ along Γ-M direction with VBM at 1.36 eV below E_F. The blue dotted lines are the calculated band structures (DFT) adapted from ref. 26, (c) Fermi surface of K doped $SnSe_2$ with conduction bands at M points. (d) Electronic structures along the momentum directions, A and B on (c). Red dots are the peaks of EDCs fitted by Gaussian function and orange curves indicate the fitted parabolic curves near the band bottom to extract the effective mass.

FIG. 1, Pham et al.

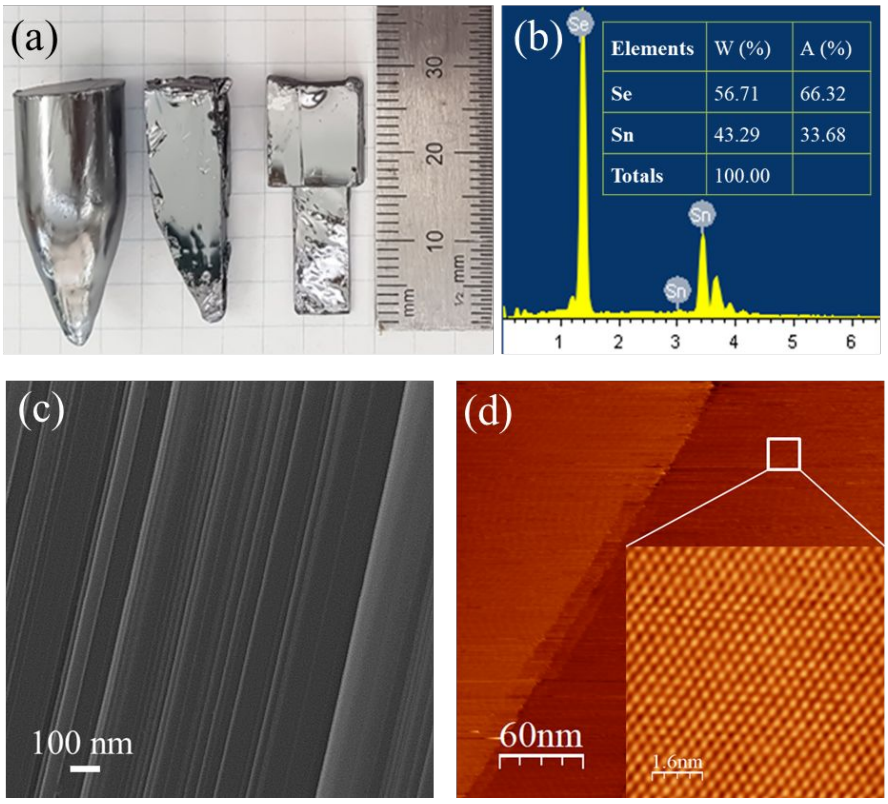

FIG. 2, Pham et al.

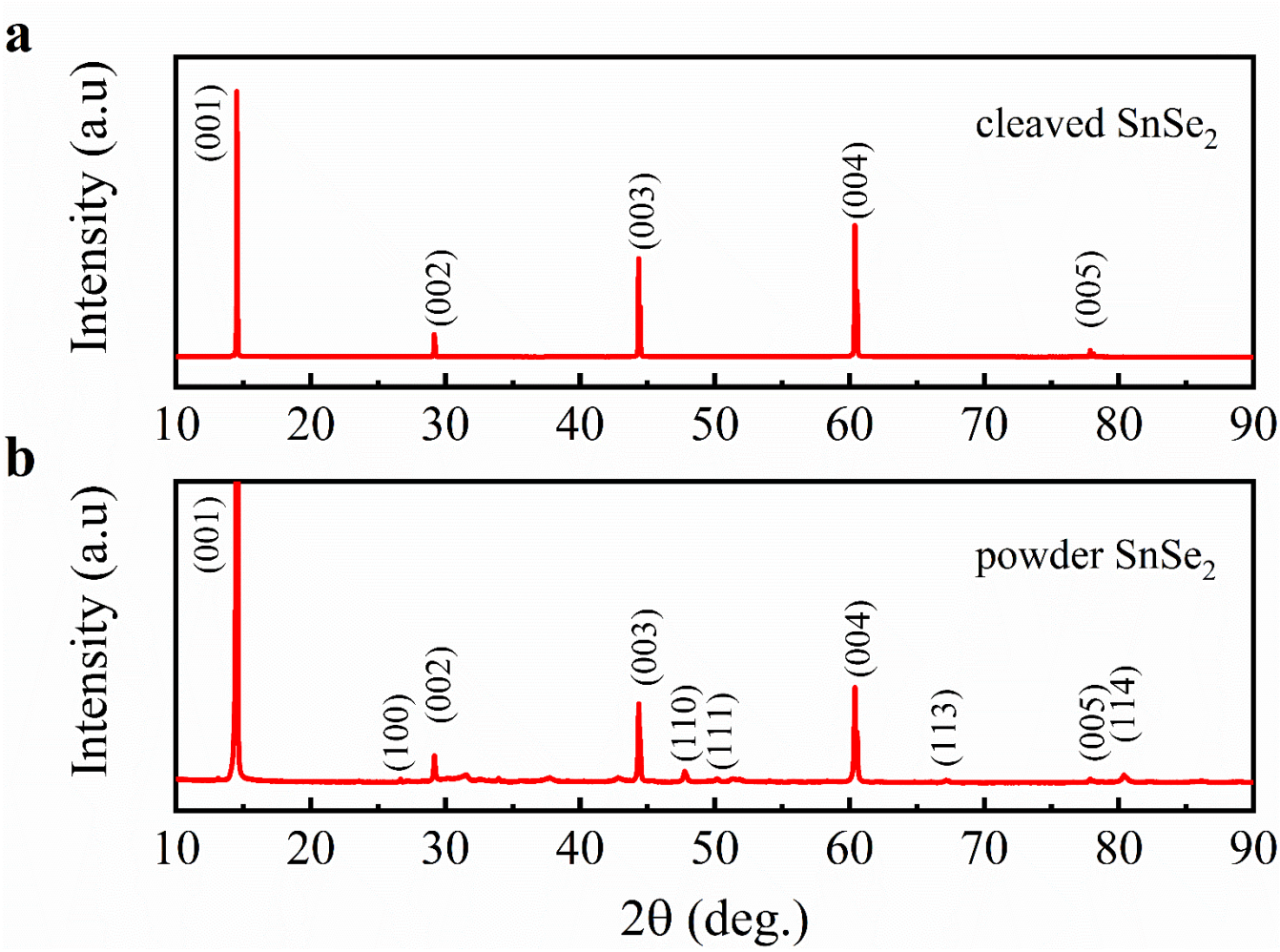

FIG. 3, Pham et al.

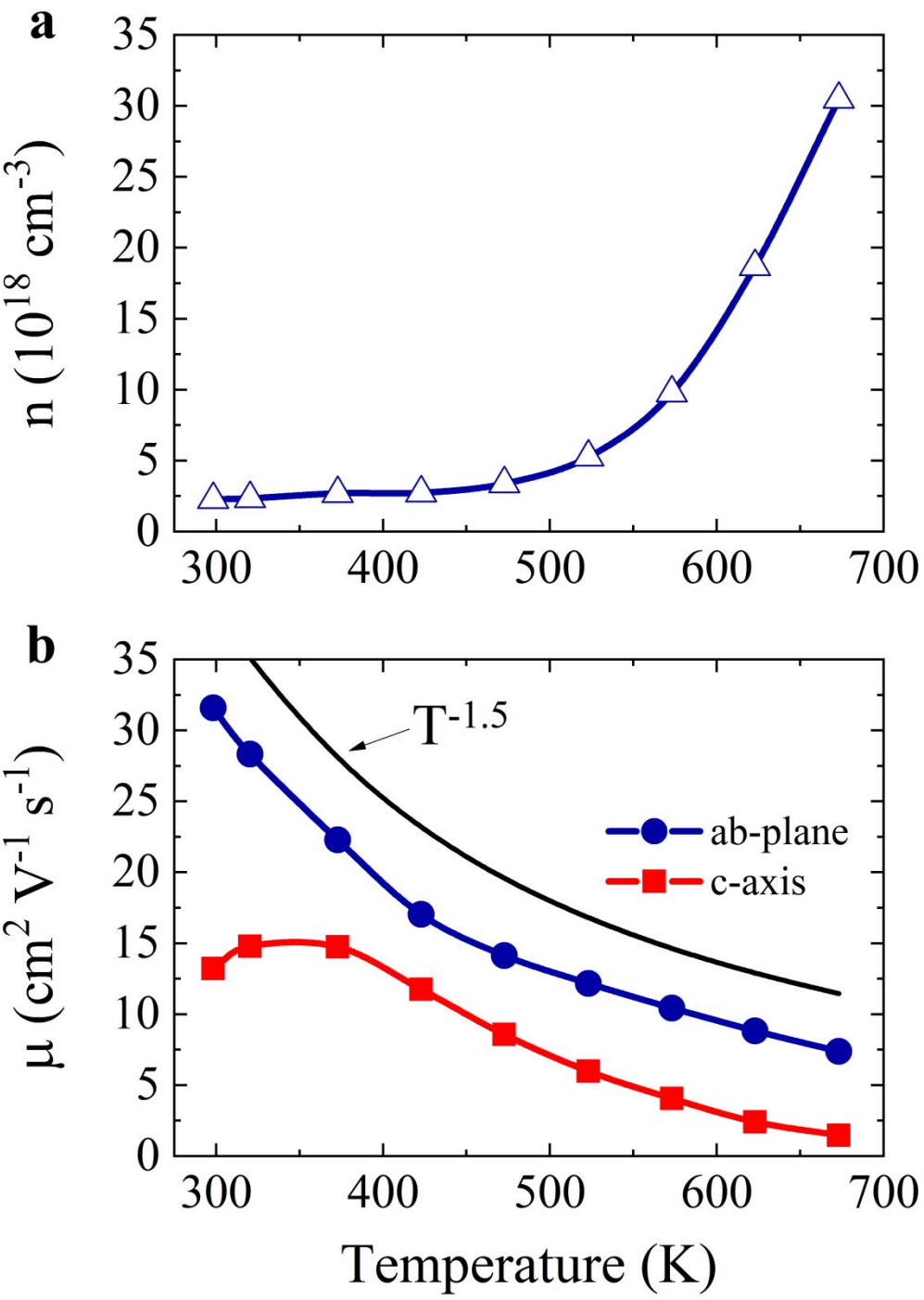

FIG. 4, Pham et al.

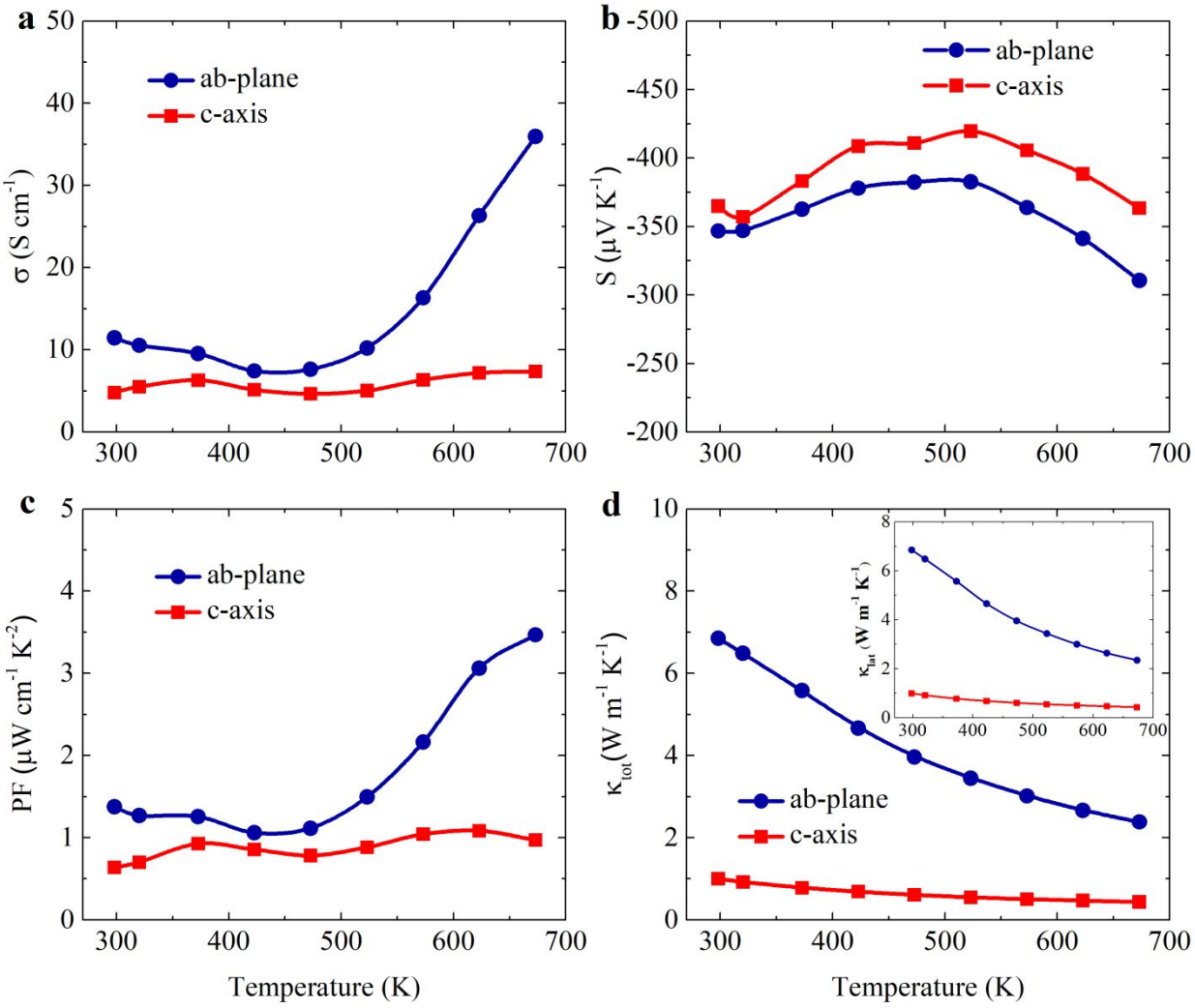

FIG. 5, Pham et al.

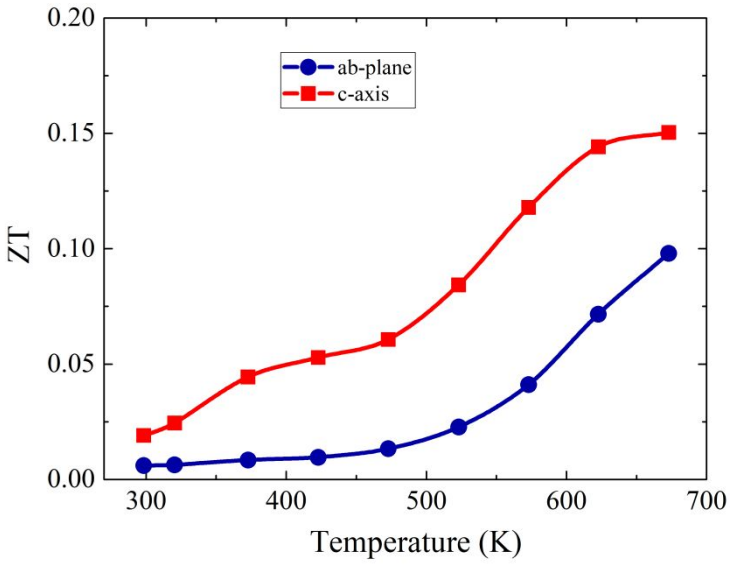

FIG. 6, Pham et al.